Econ. Environ. Geol.
Vol. 32, No. 5 p. 435-444, 1999.

# Hydrothermal Antimony Deposits of the Hyundong Mine : Geochemical Study

**Seong-Taek Yun,* Sang-Hoon Choi,** Chul-Ho Heo,* Chil-Sup So,* Gi-Tak Chae* and Ji-Wook Kim***

ABSTRACT : The antimony deposits of the Hyundong mine, located in the northeastern part of the Sobaegsan massif, occur as hydrothermal quartz+carbonate veins and stockworks which fill the fault fractures developed in Precambrian metamorphic rocks (mainly, granitic gneiss). Hydrothermal alteration occurs commonly in the vicinity of mineralized veins and is characterized by sericitization and silicification. A K-Ar age of alteration sericite is 139.2± 4.4 Ma, implying the early Cretaceous age of mineralization, possibly in association with intrusion of nearby acidic dikes (mainly, quartz porphyry). The hydrothermal mineralization occurred in five mineralization stages. These are: (1) stage I, characterized by deposition of chalcedonic quartz; (2) stage II, deposition of quartz with base-metal sulfides and stibnite; (3) stage III, deposition of quartz and carbonates (calcite, dolomite, ankerite, rhodochrosite) with various antimony-bearing minerals such as stibnite, polybasite, berthierite, native antimony, gudmundite and ullmannite; (4) stage IV, deposition of calcite with stibnite; and (5) stage V, deposition of barren calcite. Antimony occurs mostly as stibnite within stages II to IV veins, which has various habits including disseminated, veinlets and euhedral coarse crystals. Fluid inclusion studies indicate that hydrothermal mineralization at Hyundong occurred from the fluids with temperature and salinity of 330°C to 120 and 5.3 wt. % equiv. NaCl. The temperature and salinity of ore fluids systematically decreased with elapsed time in the course of mineralization, possibly due to the influx of larger amounts of meteoric groundwater. The deposition of antimony-bearing minerals occurred at low temperatures (<250°C), mainly due to the cooling and dilution of fluids. Based on the evidence of fluid boiling during the early stage II mineralization, the mineralization occurred under low pressure conditions (about 80 bars, corresponding to depths of about 350 m under hydrostatic pressure regime). Thermodynamic considerations of ore mineral assemblages indicate that antimony deposition also occurred as the results of decreases in temperature and sulfur fugacity of hydrothermal fluids. Calculated sulfur isotope composition of ore fluids ($\delta^{34}S_{\Sigma S}$=5.4 to 7.8‰) indicates an igneous source of sulfur.

## INTRODUCTION

Antimony deposits are mostly formed by hydrothermal solutions under low temperature and shallow depth conditions, and occur either as fillings in fissures and pores or as replacement ores. Epithermal veins and hot spring type deposits are characteristic. Rare antimony deposits also occur as supergene oxidation products and pegmatites. Stibnite and native antimony as principal ore minerals are typically associated with siliceous gangues and some pyrite. In complex antimony deposits, arsenopyrite, cinnabar and scheelite with varying amounts of sulfides of copper, lead, silver and zinc are also associated (Munoz, Shepherd, 1987; Munoz *et al.*, 1991; Williams-Jones, Normand, 1997).

Compared with other metallic ore deposits such as gold, lead, zinc, tungsten and molybdenum, antimony deposits are very rare in South Korea (Park, 1982; Oh, 1999). This rarity is possibly due to relatively deep crustal erosion after the episodes of metallic ore mineralization (mainly of the Mesozoic age). According to Park (1982) and Oh (1999), antimony deposits in Korea are of hydrothermal origin, occurring largely as veins and stockworks (e.g., Hyundong mine at Bongwha-Eup, Changdeok at Bonghwa-Eup, Samheung at Icheon city, and Deokseong at Cheonan city) and rarely as replacement orebobies (e.g., Wangje, Dunjeon and Baekjeon mines at Jeongseon-Eup). Previous study of antimony deposits in Korea was very scarce,

* Department of Earth and Environmental Sciences, Korea University, Seoul 136-701, Korea, Email: styun@kucc08.korea.ac.kr
** Department of Earth and Environmental Sciences, Choongbuk National University, Cheongju 361-763, Korea

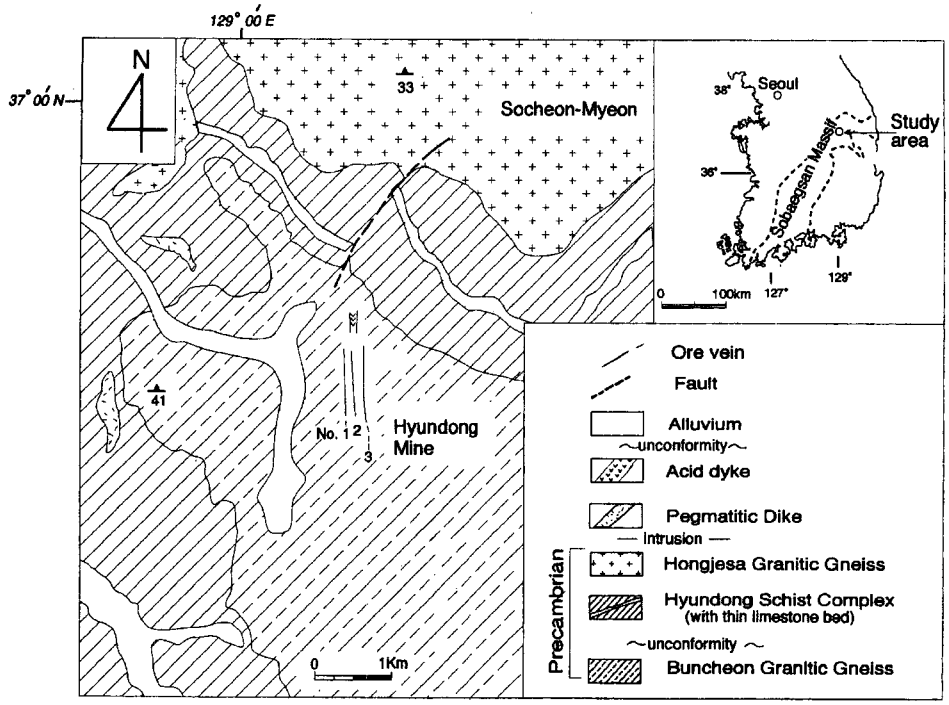


**Fig. 1.** Geologic map of the study area. In the inset, the location of the Hyundong antimony mine in the northern Sobaegsan massif is shown.

exclusively of hydrothermal replacement ores at Jeongseon area (Lee *et al.*, 1998). However, the age of antimony mineralization is not understood.

The Hyundong mine has yielded antimony ores from hydrothermal veins and stockworks after 1975, but is now closed. It is located within Precambrian metamorphic rocks of the northeastern Sobaegsan Massif (Fig. 1). Ore grades ranged widely from 0.2 to 20 wt. % Sb. Local high-grade ores have yielded 5 to 20% of antimony. Estimated ore reserves are about 2,500 metric tons of ore. There is no data on antimony mineralization of the Hyundong mine. The major purpose of this study is to elucidate the age, nature (occurrence and mineralogy) and genesis of antimony mineralization at Hyundong, in order to contribute to understand not only the antimony metallogenesis but also the temporal/spatial relationship of antimony deposits with other metallic ore deposits in Korea.

## GEOLOGIC SETTING AND ORE DEPOSITS

The Hyundong antimony mine is located approximately 200 km SEE of Seoul within the northeastern region of the Sobaegsan Massif (Fig. 1). The geology of mine area consists dominantly of Precambrian metamorphic rocks which are intruded by pegmatites and acidic dikes (Fig. 1).

The metamorphic rocks comprise the Buncheon granitic gneiss, Hyundong Schist Complex and Hongjesa granitic gneiss (Kim, Lee, 1983). The Buncheon granitic gneiss is widely distributed in the southern part of the mine area. It has the gradational contact with the Hongjesa granitic gneiss but is also locally intruded by the Hongjesa granitic gneiss. These two metamorphic rock units are largely granitic with local porphyroblastic and banded textures. The Hongjesa granitic gneiss is distributed widely in the northern part of the mine area, and consists of four rock types (granitic gneiss, leucogranitic gneiss, two-mica gneissose granite, muscovite granite; Kim, Lee, 1983). Among these rock types, the first type occurs in the mine area. The Hyundong Schist Complex was first proposed by Lee and Kim (1984) as an equivalent of the so-called "Yulri Group" which is interbedded with crystalline limestone. It has the gradational contact with the Buncheon granitic gneiss.

Pegmatites and acidic dikes ubiquitously intrude the Buncheon granitic gneiss and Hyundong Schist Complex (Fig. 1). It is noteworthy that acidic dikes frequently occur parallel in the vicinity of antimony-bearing hydrothermal veins or are cut by ore veins. This may indicate that the intusion of these acidic dikes were related to the antimony mineralization at Hyundong.

Antimony deposits of the Hyundong mine are composed of three subparallel, hydrothermal quartz+carbonates veins and stockworks (No. 1, 2, and 3 veins) which were formed by narrow open-space filling along N-S-trending fault shear zones within the Precambrian Buncheon granitic gneiss (Fig. 1). The veins commonly spray into numerous thin veinlets, forming stockworks. The No. 1 vein was the most productive with economic quantities of antimony minerals (largely stibnite). It strikes NS to N5° E, dips 80° to 85°SE, and extends to a horizontal distance of about 0.7 km along strike direction. Repeated pinching and swelling is characteristic of the No. 1 vein, and resulted in variable vein thickness (0.1 to 2 m, average=0.4 m). The No. 2 and 3 veins are similar in occurrence with the No. 1 vein.

Hydrothermal mineralization was formed through repeated fracturing and filling (at least five times) of vein, resulting in complex vein textures. The gangue minerals are changed with elapsed time as follows: chalcedonic quartz → crystalline quartz → cry-stalline quartz+carbonates (calcite, dolomite, ankerite, rhodochrosite)+fluorite → calcite. Minor amounts of sulfides such as pyrite, arsenopyrite, pyrrhotite, galena and chalcopyrite are typically associated with early quartz-rich veins. Highly silicified wallrock fragments are contained within the quartz-rich veins, typically forming chambered veins where the vein thickness increases. Economic quantities of antimony minerals occur mainly in later, carbonates quartz veins and/or stockworks which cut the quartz veins and host rocks.

Stibnite, a major antimony mineral, occurs as variable habits. These are: 1) fine-grained, disseminations or aggregates in early quartz matrix, 2) discontinuous or continuous veinlets near or along quartz vein margins, and 3) coarse (usually a few centimeters long), euhedral (prismatic or acicular) crystals within late calcite matrix.

Sericite from alteration zones yielded a K-Ar age of 139.16±4.38 Ma (Table 1). This indicates that antimony mineralization at Hyundong occurred during the Early Cretaceous.

**Table 1.** K-Ar data of alteration sericite from the Hyundong antimony deposits.

| K (%) | Radiogenic $^{40}Ar$ (moles/g) (STP×$10^{-9}$) | Radiogenic $^{40}Ar$ (%) | Date (Ma±1σ) |
|---|---|---|---|
| 7.05 | 1.768 | 71.3 | 139.16±4.38 |

## MINERAL PARAGENESIS

The deposition of hydrothermal minerals can be divided into five paragenetic stages (I, II, III, IV and V), as shown in Figs. 2 and 3. Each stage is separated by renewal of major fracturing and brecciation. Stage I represents the deposition of pre-ore chalcedonic quartz (Fig. 2A). Stage II is characterized by deposition of quartz with base-metal sulfides (Fig. 2A, B), and can be divided into two substages (IIa and IIb) on the basis of characteristic ore mineral assemblages. During the substage IIa, the majority of pyrite, arsenopyrite and sphalerite was deposited. Substage IIb is marked by deposition of pyrrhotite associated with stibnite. Stage III and IV represent the major precipitation of stibnite (Fig. 2C). Stage III occurs as quartz+carbonates veins and stockworks with various antimony minerals including stibnite, pyrargyrite, berthierite, native antimony, gudmundite and ullmannite, whereas stage IV contains only calcite as a gangue mineral and yields coarse stibnite only. Stage V occurs as post-ore barren calcite veins.

### Stage I

Stage I mineralization is characterized by the occurrence of wax-like gray chalcedony and does not contain ore minerals. Highly silicified wall-rock breccias are commonly contained within stage I veins. Stage I veins are cut by stage II and III veins, leaving as narrow discontinuous segments (Fig. 2A).

### Stage II

Stage II mineralization is characterized by the occurrence of base-metal sulfides within quartz matrix. Fragments of wall rocks and stage I veins

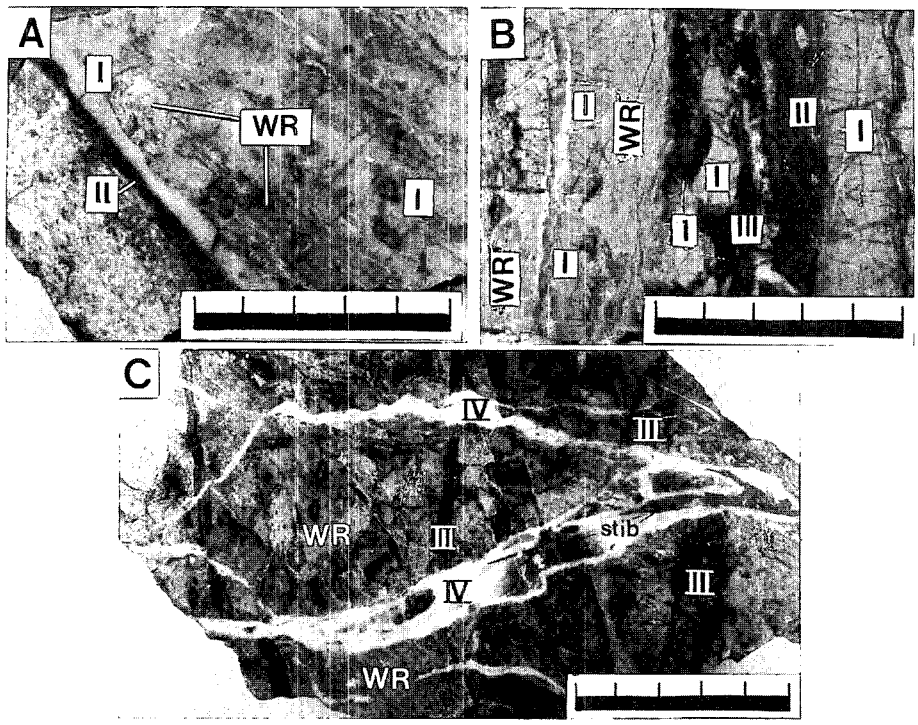


**Fig. 2.** Photographs showing the occurrence of veins of the Hyundong antimony mine. A. Stage I, gray chalcedonic quartz with wall-rock breccias (WR) are cut by stage II veins with base-metal sulfides. B. Stage I and II veins are cut by stage III veins with abundant and various antimony minerals, and are remained as breccias. Wallrock fragments (WR) are silicified and sericitized. C. Stage IV calcite veins with acicular stibnite (stib) crosscut the stage III veins and stockworks. All scale bars are 5 cm long.

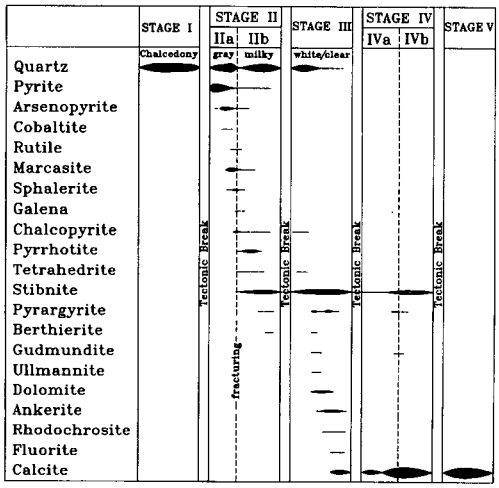


**Fig. 3.** Generalized paragenetic sequence of vein minerals from the Hyundong antimony deposits. Width of lines corresponds to relative abundance.

are often contained within stage II veins. Based on the mineralogical association, stage II mineralization can be divided into two substages (IIa and IIb; Fig. 3).

*Substage IIa* : Most of base-metal sulfides occur in substage IIa veins which are characterized by deposition of gray to transparent quartz. Hydraulic (?) fracturing occurred between the substage IIa and substage IIb.

Pyrite is predominant among base-metal sulfides and occurs as veinlets and fine- to medium-grained disseminations. It is intergrown with arsenopyrite, and is replaced by marcasite, sphalerite (5.4 to 14.1 mole % FeS), chalcopyrite and galena. Antimony minerals of substage IIb commonly penetrate the fractures of cataclastic pyrite (Fig. 4A). Fine grains of arsenopyrite (29.4~30.6 atom. % As) are intergrown with disseminated pyrites throughout the substage IIa veins, and contain cobaltites as tiny inclusions. Rutile also occurs as small (<1 mm) anhedral grains in substage IIa quartz.

*Substage IIb* : Substage IIb veins characteristically contain gray to milky quartz, pyrrhotite and

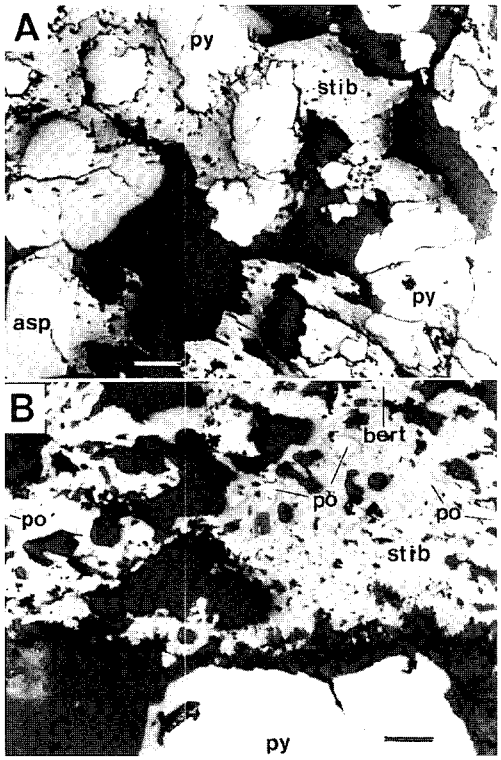


**Fig. 4.** Photomicrographs showing the occurrence of antimony minerals in veins of the Hyundong antimony mine. A. Pyrite (py) and arsenopyrite (asp) of stage IIa, which are overgrown or replaced by stibnite (stib) of stage IIb. B. Pyrrhotite (po)+berthierite (bert) assemblage of stage IIb, which is intergrown or replaced by stibnite. Scale bars are 0.1 mm long.

stibnite with minor amounts of chalcopyrite and tetrahedrite. Stibnite is dominant among ore minerals and occurs as irregular veinlets and small disseminations. It typically fills the fractures of substage IIa minerals, especially pyrite (Fig. 4A). Pyrrhotite occurs as isolated grains in substage IIb stibnite (Fig. 4B). The etching test with chromic acid shows that the pyrrhotite is monoclinic. Chalcopyrite presents as fine- to medium-sized grains intergrown with sphalerite, galena and stibnite. Tetrahedrite occurs as inclusions in sphalerite and galena, and is rarely found as fillings in fractures of chalcopyrite and stibnite.

### Stage III

Stage III is characterized by the occurrence of white to clear quartz and abundant carbonates with antimony minerals. Stage III veins and stockworks are cut by stage IV and V veins (Fig. 2C). Within stage III veins, lateral mineral zoning with the following sequence can be observed: from vein margins toward center, quartz → quartz+carbonates → carbonates+antimony minerals → antimony minerals ± calcite.

Gray, finely to coarsely crystalline carbonates are the most abundant in stage III veins. They consist of dolomite, rhodochrosite, ankerite and calcite, and form an anhedral polycrystalline aggregate locally intergrown with antimony minerals.

Economic quantities of antimony were precipitated as stibnite, pyrargyrite, berthierite, gudmundite and ullmannite during the middle to late period of stage III mineralization. Stibnite has the economic importance, and mostly occurs as prismatic crystals or irregular granular masses in carbonates. Irregular veinlets of anhedral to subhedral stibnite often cut black-colored carbonate mixture. Stibnite is rarely intergrown with pyrargyrite. Berthierite, gudmundite and ullmannite occur as tiny anhedral grains in stibnite.

### Stage IV

At the end of stage III mineralization, there was a renewal of tectonic activity which caused more faulting and brecciation. The new fractures and openings were filled by calcite, stibnite and rare berthierite. Calcite occurs as two different forms: milky white to transparent rhombohedral crystals (early), and white scalenohedral grains (late). In terms of volumetric and economic standpoints, stibnite in stage III veins are the most important. Stibnite occurs generally as prismatic to acicular grains (usually a few centimeters long) in calcite matrix (Fig. 2C). Chemical analyses of twenty stibnite samples reveal the minor amounts of arsenic with trace copper and zinc. Rare berthierite is intergrown with or replaces stibnite.

### Stage V

Stage V is characterized by deposition of barren white to pink calcite, and occurs as veins and veinlets with variable attitudes which cut the early stage veins.

## FLUID INCLUSION STUDY

About sixty samples of quartz and calcite (stages II through V) were collected for fluid inclusion study from underground ore stopes and surface. Stage I chalcedonic quartz was unsuitable for study. Microthermometric data measured include the final homogenization temperatures (Th) and ice melting temperatures (Tm-ice). Due to the small size (<8 μm) for most of inclusions, only a few Tm-ice data were obtained. The Th and Tm-ice data have standard errors of ±1.0° and ±0.2°C, respectively. Salinity data reported are based on freezing point depression in the system $H_2O$-NaCl (Bodnar, 1993). The results of fluid inclusion study are presented in Figs. 5 to 7.

The establishment of a consistent fluid inclusion chronology using normal criteria (Roedder, 1984) was frequently difficult. Therefore, we used in this study a more practical distinction between primary+ pseudosecondary (P+PS) inclusions and obvious secondary (S) inclusions. Special care was also taken to avoid stretching of fluid inclusions (especially in calcite) by the overheating.

The minerals examined contain two types of fluid inclusions ranging in size from <1 to >50 μm. These are: aqueous liquid-rich inclusions (type I), and aqueous vapor-rich inclusions (type II). Type I inclusions contain a liquid and a vapor bubble comprising 5 to 30% of the total volume of each inclusion at 25°C. They are predominant in all samples examined, and occur as both P+PS and S inclusions. Type II inclusions contain more than 80% of vapor bubble and occur only in early stage II quartz as primary inclusions. They homogenize into the vapor phase upon heating. Either any daughter minerals or traces of gas hydrates were observed in fluid inclusions.

### Microthermometric data

The P+PS inclusions in stage II quartz homogenize at temperatures from 193° to 327°C (Fig. 5). Within this temperature range, the Th data of type II inclusions are 272° to 313°C. Salinities of P+PS inclusions range from 3.4 to 5.3 equiv. wt. % NaCl (Fig. 6). A group of type I and type II inclusions occur together in early stage II quartz, and have the similar Th data. This suggests the boiling of fluid during the early periods of stage II mineralization.

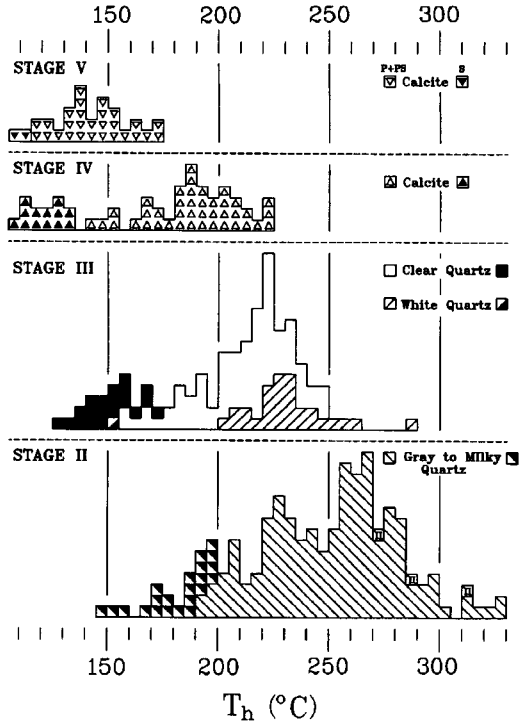


**Fig. 5.** Frequency diagrams of homogenization temperatures of fluid inclusions in vein minerals from the Hyundong antimony deposits. There is a general decrease of temperature with elapsed time. P+PS=primary and pseudosecondary; S=secondary; II=aqueous vapor-rich inclusions.

White or clear quartz from stage III veins contains type I inclusions only. The Th data of P+PS inclusions range from 156° to 287°C (white quartz, 202°~287°C; clear quartz, 156°~249°C). Their salinities range from 2.4 to 4.4 equiv. wt. % NaCl (Figs. 5 and 6).

Stage IV calcites contain only type I inclusions (mostly, <10 μm in size). The vapor bubbles comprise <20 volume % of the inclusion. The Th and salinity data of P+PS inclusions are 142° to 223°C and 1.1 to 2.6 equiv. wt. % NaCl, respectively. Primary type I inclusions in stage V calcites homogenize at temperatures of 117° to 173°C, and have the salinities of 0.9 to 1.3 equiv. wt. % NaCl (Figs. 5 and 6).

### Thermal and compositional variation of hydrothermal fluids

Histograms of Th data of fluid inclusions (Fig.

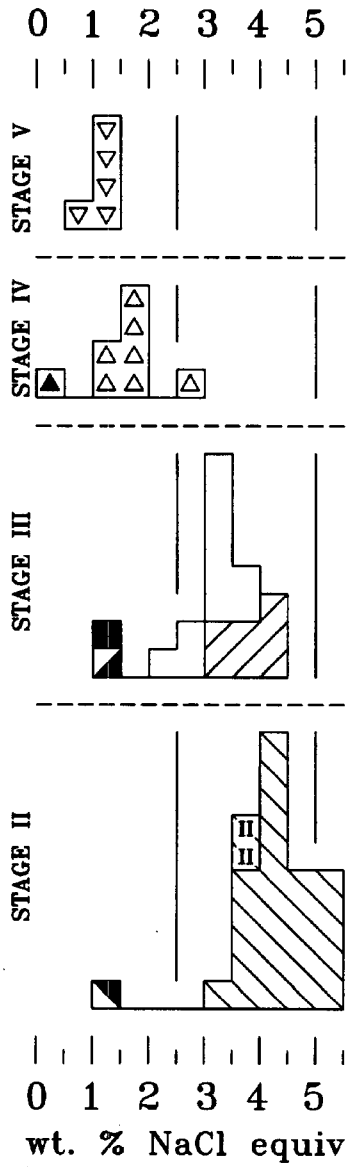


**Fig. 6.** Frequency diagrams of salinities of fluid inclusions in vein minerals from the Hyundong antimony deposits. There is a general decrease of salinity with elapsed time. Symbols are the same as in Fig. 5.

5) show a progressive decrease of temperature with increasing paragenetic time during the mineralization at Hyundong. Deposition of antimony in stages II to IV also occurred as a result of the temperature decrease (in average temperature, from about 260° to 140°C; Fig. 5). The deposition of latest barren calcite in stage V occurred at temperatures down to 115~175°C.

The salinity data also show a systematic decrease with elapsed time, from about 5.5 to <1 wt. % NaCl (Fig. 6). Therefore, we consider that the hydrothermal system at Hyundong was repeatedly inundated by progressively larger volumes of cooler and dilute waters (meteoric water?).

The relationship between Th and salinity data for stage II (Fig. 7) suggests a complex history of boiling, cooling and dilution. During the early period with temperatures of >250°C within stage II, boiling of the fluids led to slight increase in salinity. After the boling, the simple cooling and dilution of fluids resulted in decreasing salinity with decreasing temperature (Fig. 7). The positive arrays of data plots for stages III and IV (Fig. 7) also indicate the progressive cooling and dilution of hydrothermal fluids, likely due to repeated fracturing events allowing dilute meteoric waters into the hydrothermal system. By the advent of stage V, cooling and dilution of hydrothermal fluids were pronounced.

In summary, Fig. 7 indicates that deposition of Fe- and base-metal sulfides in early period of stage II resulted from boiling of hydrothermal fluids. On the other hand, deposition of antimony minerals in the time span from late period of stage II to stage IV occurred at temperatures of <250°C mainly as a result of progressive cooling and dilution of hydrothermal fluids.

### Pressure-depth consideration

As described above, the coexistence of type I inclusions with type II inclusions in early period of stage II indicate the occurrence of boiling of hydrothermal fluids. The P-T-X data for the boiling conditions for the system $H_2O$-NaCl (Haas, 1971), combined with temperature and salinity data for these inclusions, suggest the pressures of about 80 bars. The pressures correspond to shallow crustal depths (around 350 m) for the mineralization under hydrostatic pressure regime.

## GEOCHEMICAL ENVIRONMENT OF ANTIMONY DEPOSITION

Equilibrium thermodynamic consideration was made to estimate the changes in geochemical con-

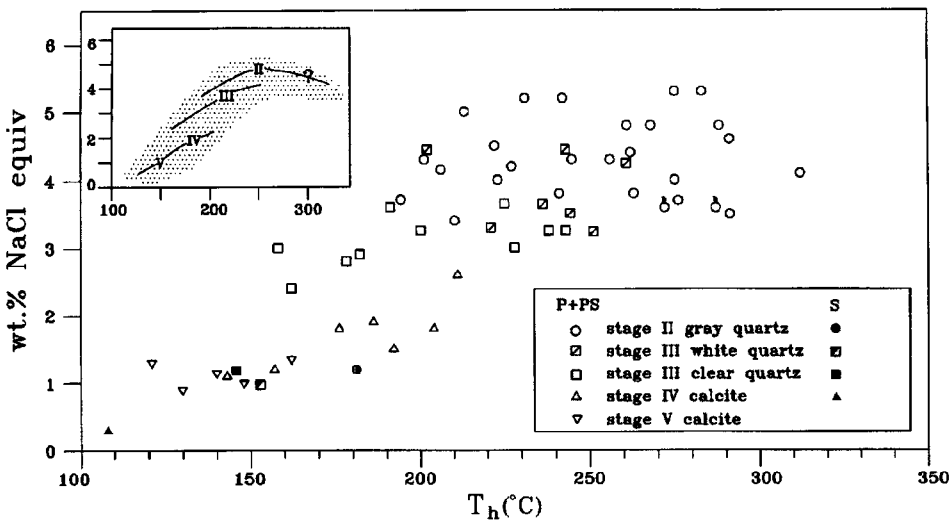


**Fig. 7.** Homogenization temperature versus salinity diagram for fluid inclusions in vein minerals from the Hyundong antimony deposits. In the inset, probable evolution of hydrothermal fluids are shown as arrows. P+PS=primary and pseudosecondary; S=secondary.

ditions of hydrothermal fluids during the antimony deposition in stages II to IV. The phase relations and mineral compositions in the systems Fe-Zn-S, Fe-As-S, Ag-Sb-S, Ag-Fe-Sb-S and Fe-Sb-S (Barton, 1971; Scott, Barnes, 1971; Craig, Barton, 1973; Kretschmar, Scott, 1976) were used to trace the changes in temperature and sulfur fugacity ($fs_2$), as shown in Fig. 8.

The assemblage pyrite+sphalerite ($X_{FeS}$=0.05-0.14) ±arsenopyrite (<30.6 atom. % As) in the pre-antimony, base metal-rich substage IIa mineralization was precipitated at temperatures between 250° and 300°C from the fluids with log $fs_2$ values of -10.5 to -13.5 atm (Fig. 8). Within the substage IIb, Sb(Ag-Fe)-bearing minerals were deposited with monoclinic pyrrhotite. This substage IIb assemblage indicates the lower values of temperature (about 250° to 200°C) and $fs_2$ ($10^{-13.5}$ to $10^{-17}$) than those for substage IIa (Fig. 8). This indicates that deposition of antimony minerals (stibnite, pyrargyrite, berthierite and tetrahedrite) in substage IIb was a result of decreases in temperature and sulfur fugacity, likely due to mixing with meteoric waters.

Within stages III and IV, various kinds of antimony-bearing sulfide (stibnite) and sulfosalts (pyrargyrite, berthierite, gudmundite, ullmannite) were precipitated together with quartz or carbonates. The probable conditions of temperature and $fs_2$ for stages III and IV can be set by intersecting the

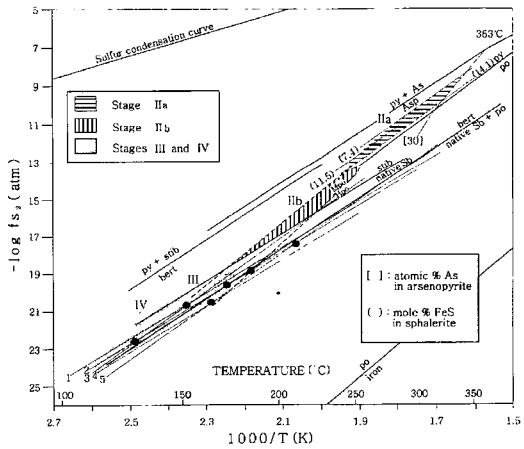


**Fig. 8.** Temperature versus fugacity of sulfur ($fs_2$) diagram showing sulfidation reactions pertinent to ore mineral assemblages of the Hyundong antimony deposits. Probable depositional conditions of each stage are shown as hatched or shaded regions. The numbered sulfidation reaction curves are: 1; pyrargyrite+native antimony+$S_2$ ↔ miargyrite (Craig, Barton, 1973); 2; argentite+native antimony+$S_2$ ↔ miargyrite (Craig, Barton, 1973); 3; gudmundite+$S_2$ ↔ pyrite+native antimony (Barton, 1971); 4; argentite+native antimony+$S_2$ ↔ pyrargyrite (Craig, Barton, 1973); 5; pyrargyrite+ pyrrhotite+ native antimony+$S_2$ ↔ miargyrite+gudmundite (Craig, Barton, 1973). Abbreviations: As; native arsenic, Asp; arsenopyrite, bert; berthierite, hpo; hexagonal pyrrhotite, mpo; monoclinic pyrrhotite, po; pyrrhotite, py; pyrite, stib; stibnite.

appropriate sulfidation reaction curves, as shown in Fig. 8. The maximum values of estimated tem-

**Table 2.** Sulfur isotope data of sulfides from the Hyundong antimony deposits.

| Sample no. | Mineral | Stage | $\delta^{34}S$ (‰) | T (°C)[1)] | $\delta^{34}S_{H2S}$ (‰) |
|---|---|---|---|---|---|
| HD-40-1 | pyrite | IIa | 6.8 | 290 | 5.5 |
| HD-40-2 | pyrite | IIa | 6.7 | 280 | 5.4 |
| HD-42 | pyrite | IIa | 6.8 | 280 | 5.5 |
| HD-33 | stibnite | IIb | 3.9 | 220 | 7.0 |
| HD-15-1 | stibnite | IV | 3.8 | 180 | 7.5 |
| HD-41 | stibnite | IV | 3.8 | 160 | 7.8 |

[1)] Temperature estimates based on fluid inclusions and thermodynamic considerations of ore mineral assemblages.
[2)] Calculated using sulfur isotope fractionation equations compiled by Ohmoto, Rye (1979).

perature and $fs_2$ conditions are less than 200°C and $10^{-17.0}$ atm, respectively.

It is noteworthy that temperatures estimated for each stage agree well with homogenization temperatures of fluid inclusions. The agreement of temperatures estimated each based on mineral assemblages and fluid inclusions also suggests the low pressure and shallow depth conditions of hydrothermal mineralization at Hyundong (Potter, 1977). Fig. 8 also shows the general decreases in temperature and $fs_2$ of hydrothermal fluids with elapsed time.

## SULFUR ISOTOPE STUDY

We have measured sulfur isotope compositions of six sulfides (pyrite and stibnite) from the Hyundong mine (Table 2). Standard techniques for extraction and analysis were used as described by Grinenko (1962). Isotope data are reported in standard δ notation relative to the Canyon Diablo Troilite (CDT) standard, and have the standard analytical error of about ±0.1‰.

Three pyrites from stage IIa veins have the uniform $\delta^{34}S$ values ranging from 6.7 to 6.8‰, whereas three stibnites from stage IIb and IV have the values of 3.8 to 3.9‰ (Table 2). Assuming depositional temperatures of >250°C for stage IIa pyrites, 200~250°C for stage IIb stibnites, and 150~220°C for stage IV stibnites (based on temperatures estimated from mineral assemblages and fluid inclusions, along with paragenetic constraints), the $\delta^{34}S$ values of $H_2S$ in hydrothermal fluids are calculated as follows (Table 2): stage IIa, 5.4-5.5‰; stage IIb, 7.0‰; and stage IV, 7.5~7.8‰. There is an apparent increase in $\delta^{34}S$ values of $H_2S$ with elapsed time. Within stage II, both the ore mineral assemblage pyrite+pyrrhotite without any oxide mineral and the alteration assemblage sericite+quartz in or near veins suggest that dissolved sulfur in stage II fluids were present dominantly as reduced forms ($H_2S$ and $HS^-$). Therefore, the calculated $\delta^{34}S_{H2S}$ values for stage II fluids (5.4~7.0‰) may be taken as the sulfur isotope composition of entire hydrothermal fluids ($\delta^{34}S_{\Sigma S}$) and may indicate an igneous source of sulfur (Ohmoto, Goldhaber, 1997).

## ACKNOWLEDGMENTS

This research was financially supported by the Center for Mineral Resources Research, Korea University.

## REFERENCES

Barton, P.B., Jr. (1971) The Fe-Sb-S system. Econ. Geol., v. 66, p. 121-132.

Bodnar, R.J. (1993) Revised equation and table for determining the freezing point depression of $H_2O$-NaCl solutions. Geochim. Cosmochim. Acta, v. 57, p. 683-684.

Craig, J.R. and Barton, P.B., Jr. (1973) Thermochemical approximations for sulfosalts. Econ. Geol., v. 68, p. 493-506.

Grinenko, V.A. (1962) Preparation of sulfur dioxide for isotopic analysis. Zeitschr. Neorgan. Khimii, v. 7, p. 2478-2483.

Haas, J.L. (1971) The effect of salinity on the maximum thermal gradient of a hydrothermal system at hydrostatic pressure. Econ. Geol., v. 66, p. 940-946.

Kim, Y.J. and Lee, D.S. (1983) Geochronology and petrogenetic processes of the so-called Hongjesa Granite in the Seokpo-Deogku area. Jour. Korean Inst. Mining Geol., v. 16, p. 163-221 (in Korean).

Kretschmar, U. and Scott, S.D. (1976) Phase relations involving arsenopyrite in the system Fe-As-S and their application. Am. Mineral., v. 14, p. 364-386.

Lee, C.H., Choi, S.W., Hur, S.D. and Hwang, J. (1998) Epithermal mineralization of the Wangje antimony deposit, Korea: geochemistry and mineralogy. Jour. Geol. Soc. Korea, v. 34, p. 228-242 (in Korean).

Lee, S.M. and Kim, H.S. (1984) Metamorphic studies on the so-called Yulri and Weonnam Groups in the Mt.

Taebaeg area. Jour. Geol. Soc. Korea, v. 20, p. 195-214 (in Korean).

Munoz, M. and Shepherd, T.J. (1987) Fluid inclusion study of the Bournac polymetallic (Sb-As-Pb-Zn-Fe-Cu...) vein deposit (Montagne Noire, France). Mineral. Deposita, v. 22, p. 11-17.

Munoz, M., Courjault-Rade, P., Tollon, F., Fortune, J.P. and Belhaj, O. (1991) The massive stibnite lode-deposits of the French Paleozoic basement. Evaluation of physico-chemical factors for stibnite precipitation from thermodynamic modelling. In: Pagel, M. and Leroy, J.L. (eds.). Sources, transport and deposition of metals, Rotterdam, A.A. Balkema, p. 205-208.

Oh, M.S. (1999) Ore mineralization. In: Geological Society of Korea (ed.). Geology of Korea, Seoul, Sigma Press, p. 596-598 (in Korean).

Ohmoto, H. and Goldhaber, M.B. (1997) Sulfur and carbon isotopes. In: Barnes, H.L. (ed.). Geochemistry of Hydrothermal Ore Deposits (3rd ed.), New York, Wiley Intersci., p. 517-611.

Ohmoto, H. and Rye, R. O. (1979) Isotopes of sulfur and carbon, In: Barnes, H.L. (ed.). Geochemistry of Hydrothermal Ore Deposits (2nd ed.), New York, Wiley Intersci., p. 509-567.

Park, H.I. (1982) Metallic ore deposits. In: Geology and Mineral Resources of Korea, Department of Geology Alumni of Yonsei University, Seoul, p. 330-331 (in Korean).

Potter, R.W. III. (1977) Pressure corrections for fluid inclusions homogenization temperatures based on the volumetric properties of the system NaCl-$H_2O$. Jour. Res. U.S. Geol. Survey, v. 5, p. 603-607.

Roedder, E. (1984) Fluid inclusions. Rev. Mineralogy, v. 12, 664 p.

Scott, S.D. and Barnes, H.L. (1971) Sphalerite geothermometry. Econ. Geol., v. 66, p. 653-669.

Williams-Jones, A.E. and Normand, C. (1997) Controls of mineral paragenesis in the system Fe-Sb-S-O. Econ. Geol., v. 92, p. 308-324.

1999년 6월 16일 원고접수, 1999년 7월 28일 게재승인.

# 현동 광산의 열수 안티모니 광화작용 : 지화학적 연구

윤성택 · 최상훈 · 허철호 · 소칠섭 · 채기탁 · 김지욱

**요 약** : 현동 안티모니 광상은 소백산 육괴의 북동부 지역에 위치하며, 선캠브리아기 변성암류(주로 화강암질 편마암)에 발달하는 단층 열극을 충진한 석영+탄산염 광맥 및 망상맥으로 산출된다. 광맥 인접부에는 견운모화 및 규화 작용으로 특징되는 열수 변질대가 발달한다. 변질대 견운모의 K-Ar 연령은 139.2±4.4 Ma로서 백악기초의 광화 시기를 나타내는데, 광화작용은 산성 암맥(주로 석영 반암)의 관입과 관련되었으리라 사료된다. 열수 광화작용은 5회에 걸쳐 진행되었다. 광화 1기에는 옥수질 석영이 침전하였으며, 광화 2기에는 천금속(base-metal) 황화 광물 및 휘안석을 수반한 석영맥이 형성되었다. 광화 3기에는 휘안석, 농홍은석, 버티어라이트, 자연 안티모니, 구드문다이트, 울마나이트 등 다양한 함안티모니 광물이 석영 및 탄산염 광물(방해석, 돌로마이트, 앵커라이트, 능망간석)에 수반되어 정출되었다. 광화 4기에는 휘안석을 수반한 방해석이, 그리고 광화 5기에는 barren한 방해석이 침전하였다. 안티모니는 광화 2기에서 4기에 걸쳐 주로 휘안석으로 산출되며, 산점상, 세맥상 및 조립질 자형 결정 등 다양한 형태를 갖는다. 유체 포유물 연구에 의하면, 열수 광화작용은 ≤ 5.3 wt. % NaCl 상당 염농도의 유체로부터 120~330°C의 온도에서 진행되었다. 광화 유체의 온도 및 염농도는 광화작용의 진행과 더불어 점진적으로 감소하였는데, 이는 열수계 내로 다량의 순환 강우가 유입되었음을 지시한다. 함안티모니 광물의 침전은 비교적 저온(<250°C)에서 주로 유체의 냉각 및 희석 작용에 의해 진행되었다. 광화 2기 초기에서 인지되는 유체의 비등 현상에 의하여, 광화작용의 압력은 비교적 낮았음(정수압 조건에서 약 350 m의 심도에 해당하는 약 80 bar)을 알 수 있다. 광석광물의 조합에 대한 열역학적 고찰 결과, 안티모니 침전은 열수 유체의 온도 및 유황 분압의 감소에 기인하였다. 광화 유체의 황동위원소 조성($\delta^{34}S_{\Sigma S}$)은 5.4~7.8‰이었으며, 이는 화성 기원을 지시한다.